CFD COMPUTATIONS OF LIQUID HYDROGEN RELEASES

Ichard, M.[1], Hansen, O.R.[1] , Middha, P.[1] and Willoughby, D.[2]
[1] GexCon AS, P.O. Box 6015, Postterminalen, Bergen, NO-5892, Norway, mathieu@gexcon.com
[2] Health and Safety Laboratory, Harpur Hill, Buxton, Derbyshire SK17 9JN, United Kingdom, Deborah.Willoughby@hsl.gov.uk

ABSTRACT

Hydrogen is widely recognized as an attractive energy carrier due to its low-level air pollution and its high mass-related energy density. However, its wide flammability range and high burning velocity present a potentially significant hazard. A significant fraction of hydrogen is stored and transported as a cryogenic liquid (liquid hydrogen, or LH_2) as it requires much less volume compared to gaseous hydrogen. In order to exist as a liquid, H_2 must be cooled to a very low temperature, 20.28 K. LH_2 is a common liquid fuel for rocket applications. It can also be used as the fuel storage in an internal combustion engine or fuel cell for transport applications. Models for handling liquid releases, both two-phase flashing jets and pool spills, have been developed in the CFD-model FLACS. The very low normal boiling point of hydrogen (20K) leads to particular challenges as this is significantly lower than the boiling points of oxygen (90K) and nitrogen (77K). Therefore, a release of liquid hydrogen in the atmosphere may induce partial condensation or even freezing of the oxygen and nitrogen present in the air. In our computations of two-phase jets we assume that the dispersed and continuous phases are in thermodynamic and kinematic equilibrium. A pool model is used to compute the spreading and vaporization of the liquid hydrogen depositing on the ground and also the partial condensation or freezing of the oxygen and nitrogen is taken into account. Simulations with the new models will be compared against selected experiments performed at the Health and Safety Laboratory (HSL)

1.0 INTRODUCTION AND PREVIOUS WORK

Even though liquid hydrogen tanks can store more fuel in a given volume than compressed hydrogen tanks, there are several downsides to using liquid hydrogen to power large vehicles. One concern is that unintended releases (loss of containment) of cryogenic liquids such as LH_2 from pressurized or non-pressurized storage tanks may form a potentially dense hazardous gas cloud. Such a release could also damage important infrastructure around the release due to the low temperatures. Accurate hazard assessments of storage systems require a proper prediction of the two-phase jet dispersion (if the tank is pressurized), liquid hydrogen pool evaporation and spreading. Very few releases of limited size will create a pool, as the liquid hydrogen will evaporate immediately as it comes into contact with surfaces. In the cases where a pool is formed, it is necessary to properly model the spill motion and evaporation rate to get a good description of the gas cloud. Another issue that requires attention is the atmospheric flow field. The terrain, vegetation and buildings will influence the flow field, which only in a few exceptional cases can be considered uniform. This emphasizes the need for a Computational Fluid Dynamics (CFD) tool to calculate dispersion of the gas cloud and, furthermore, a local formulation of the mass and heat transfer between the hydrogen cloud and the surrounding flow.

FLACS has been validated against large-scale liquid H_2 release and dispersion experiments [1]. One of the simulated experiments was performed by Battelle Ingenieurtechnik and Bundesanstalt fur Materialforschung und Prufung (BAM), Berlin, in the frame of the Euro-Quebec-Hydro-Hydrogen-Pilot-Project and dealt mainly with LH_2 near ground releases between buildings [2]. The experimental trial 5 was used for simulation due to the fact that in this release the largest numbers of sensor readings were obtained. The release occurred between two buildings and Ref. [2] reported an estimated release rate of LH_2 of 0.37 kg/s that lasted for 125 s. A neutral stability class has been used in the simulations and the estimated average wind speed was 0.5 m/s at a height of 0.9 m. The simulated results compared reasonably well with experimental data.

FLACS has also been applied to the simulation of the NASA release experiments. These experiments involving large-scale releases of liquefied hydrogen were carried out at White Sands, New Mexico in the early part of 1980s [3,4]. The experiments aimed to investigate the generation and dispersion of flammable clouds that could be formed as a result of large, rapid spills of liquid hydrogen. The experiments consisted of spills of up to 5.7 m^3 of liquid hydrogen (~ 402 kg), with spill durations of approximately 35 seconds. The validation work used results for test 6. These experiments have also been previously modelled [5,6]. FLACS provided a good agreement with experimental data for evaporation rate and pool radius. Since no information about the atmospheric stability classes was available, simulations were performed by using the stable and neutral stability classes. Time series of gas concentrations showed that the atmospheric stratification was a key parameter in the dispersion of the hydrogen plume. The stable configuration gave the most coherent results when compared to experimental observations.

It is also worth mentioning that recently FLACS has been validated against the experiments of the model evaluation database of the Model Evaluation Protocol [7]. The stated purpose of the MEP is to "provide a comprehensive methodology for determining the suitability of models to accurately simulate the dispersion of vapours emanating from accidental spills of LNG on land". More than 30 experiments of dense gas dispersion in obstructed and non-obstructed terrain have been simulated [8]. The MEP defines a set of statistical performance measures (SPM) that need to be calculated in order to provide a quantitative assessment of the capability of a model to "predict reality". FLACS successfully meets the quantitative criteria for LNG vapour dispersion model validation as established in the MEP. Validation work on flashing jets have also been performed in the last two-years. A two-phase module has been implemented in FLACS where we assume that the dispersed and continuous phases are in thermodynamic and kinematic equilibrium. A pool model is used to compute the spreading and vaporization of the liquid depositing on the ground. The FLIE-INERIS propane and butane flashing jets have been simulated and the results for the temperature profiles along the centre-line axis of the jet compare well with experimental observations [9]. The Desert-Tortoise test series (ammonia flashing jets) have also been considered and the concentration time-series predicted by FLACS were shown to be in good agreement with the experimental data [10].

This paper is organized as follows: The FLACS CFD model is presented in Section 2 which contained three sub-sections. In the first sub-section, Section 2.1, we describe the atmospheric dispersion model; in Section 2.2 we detail the Homogeneous Equilibrium Model (HEM) and its implementation in FLACS; in Section 2.3, we present the model for liquid deposition on the ground (rain-out) and the pool model. Finally in Section 3, we describe the experimental tests and compare our predictions with the experimental observations. The conclusions of this work are given in Section 4.

2.0 THE FLACS CFD MODEL

2.1 The atmospheric dispersion model

FLACS is a specialized CFD tool developed to address process safety applications such as:

- Dispersion of flammable or toxic gases;
- Gas and dust explosions;
- Propagation of blast and shock waves;
- Pool and jet fires.

FLACS calculates the atmospheric dispersion of gases and vapours by solving the three-dimensional (3D) Reynolds-averaged Navier Stokes (RANS) equations on a non-uniform Cartesian grid, with the standard k-ε model for turbulent closure [11]. Unlike most other commercial CFD models, FLACS uses the distributed porosity concept [12] to handle sub-grid objects (i.e., objects that are smaller than the grid cell size). This approach allows the simulation of dispersion in complex geometries accurately and at much smaller computational costs than other CFD codes. For atmospheric dispersion

simulations, the atmospheric boundary layer is modelled by imposing profiles for velocity, temperature and turbulence on flow inlet boundaries. These profiles are specified as a function of the atmospheric stability (expressed according to the Pasquill-Gifford stability classes) and the surface roughness length, z_0. Logarithmic velocity profiles follow the derivation by van den Bosch [13] and can be written as:

$$U(z) = \frac{u_*}{\kappa}\left(\ln\left(\frac{z}{z_0}\right) - \psi_m\right) \tag{1}$$

where the friction velocity u* is given by:

$$u_* = \frac{U_0 \kappa}{\ln\left(\frac{z_{ref}}{z_0}\right) - \psi_m} \tag{2}$$

where U_0 is the velocity at the reference height z_{ref} . The stability function ψ_m is also given by van den Bosch (van den Bosch & Weterings, 1997) as:

$$\psi_m = \begin{cases} 2\ln\left(\frac{1+\xi}{2}\right) + \ln\left(\frac{1+\xi^2}{2}\right) - 2\arctan\left(\xi\right) + \frac{\pi}{2} & \text{for } L < 0 \\ -17\left(1 - \exp\left(-0.29\frac{z}{L}\right)\right) & \text{for } L > 0 \end{cases} \tag{3}$$

where $\xi = \left(1 - 16\, z/L\right)^{1/4}$.

The temperature profile is assumed uniform. The expressions for the turbulent kinetic energy (k) and turbulence dissipation rate (ε) for neutral and stable atmospheric boundary layers are given by Han et *al.* [14]

Further model details can be found elsewhere [1,8]. The atmospheric dispersion model in FLACS has been tested for a wide range of scenarios including releases of dense, passive and buoyant gases in open, obstructed and enclosed spaces [1,15-18].

2.2 The Homogeneous Equilibrium Model

The Homogeneous Equilibrium Model (HEM) is a simplified approach for modelling two-phase flows where it is assumed that both phases are in local thermal and kinematic equilibrium. It implies that the transport between the phases is infinitely fast. This approach only distinguishes the two phases by their volume (or mass) fractions in a given mixed volume. The temperature, velocity and other flow field parameters are the same for the two phases and the denomination mixture temperature or mixture velocity is often encountered.

The HEM approach has two main advantages:

- It requires limited information about the source (see below).
- The conservation equations are similar to single phase flow conservation equations.

The approach does not require information about the particle diameter and velocity at the source. The particle volume fraction is the only parameter needed to characterize the dispersed phase at the source.

This can be seen as an advantage because a lot of uncertainties remain in estimating the characteristics of particles produced by the atomization of liquid sprays (despite some recent efforts, see for example [19,20]). The second bullet implies that minor modifications to single phase flow CFD codes (such as FLACS) are needed. These modifications are detailed in the next paragraph.

The main disadvantage of the HEM approach is due to the equilibrium, infinitely fast transfer, assumption which seems to fail for large particle diameters. Kukkonen et *al.* [21] used the HEM approach to compute the dispersion of two-phase ammonia jets and they assessed the performances of the HEM approach by comparing the results with a more advanced two-phase flow model (the model was based on Lagrangian particle tracking). They found that the results were identical (within 1%) when the ammonia droplets had a diameter smaller than 100 microns. Faeth [22] provides a thorough theoretical description of the HEM approach and reports comparisons between HEM predictions and experiments for evaporating and combusting sprays. Both Refs. [21] and [22] conclude that the finite inter-phase transport rates account for much of the differences between the HEM approach and experimental observations.

Some details about the implementation of the HEM method inside the FLACS CFD model are now discussed. In each grid cell the calculations must provide the mass fractions of air, contaminant in the gas phase and contaminant in the liquid phase. The mass fractions are related to the mixture fraction and the initial mass fractions via the following equation:

$$\begin{cases} Y_i = Y_{i_0}^a + f_g Y_{i_0}^g + f_l Y_{i_0}^l \\ \sum_i Y_i = 1 \end{cases} \tag{4}$$

where Y_i is the mass fraction of element i at a given location $\vec{x}$. In the current paper we are dealing with releases of liquid hydrogen and therefore the elements present are: O_2, N_2, H_2-vapor and H_2-liquid. In Equation 4, $Y_{i_0}^a$ is the initial mass fraction of element i inside the surrounding atmosphere, $Y_{i_0}^g$ is the initial mass fraction of element i inside the gas phase at the source, and $Y_{i_0}^l$ is the initial mass fraction of element i inside the liquid phase at the source. Transport equations are solved for the two mixture fractions f_g and f_l (the index $*$ represents g or l):

$$\frac{\partial \rho f_*}{\partial t} + \frac{\partial \rho u_j f_*}{\partial x_j} = \frac{\partial}{\partial x_j}\left(\frac{\mu_t}{\sigma_{f_*}} \frac{\partial f_*}{\partial x_j} \right) + S_{f_*} \tag{5}$$

The mixture fraction $f_*\left(x_j, t\right)$ indicates how much of the quantity $Y_{i_0}^*$ has been transported to the location x_j at time t. The source term S_{f_*} contains the effects of the evaporation and eventual deposition on the ground of the liquid phase. A similar transport equation is solved for the mixture enthalpy with source term S_h represents the loss of energy due to liquid deposition. Evaporation of the liquid phase is taken into account by ensuring thermodynamic equilibrium in each grid cell. Thermodynamic equilibrium implies that the partial pressure of the contaminant in the vapour phase is the saturation pressure at the mixture temperature. The partial pressure of the contaminant vapour is deduced from the Dalton's law

$$P_g = \alpha_g P_{atm} = P_{sat}(T) \tag{6}$$

where α_g is the volume fraction of the contaminant vapour. We iterate on the temperature until equilibrium is attained. Equilibrium is attained when the enthalpy is equal to the initial enthalpy in the control volume. The same method is employed to estimate the amount of oxygen and nitrogen that

condensates in grid cells where the temperature is less than their boiling points. The condensation process releases energy, i.e. the temperature of the mixture increases, whereas the evaporation process cools down the mixture.

2.3. The rain-out and pool models

A model to estimate the amount of liquid that deposits on the ground is proposed and has been implemented inside the FLACS CFD model. Rain-out is due to jet impingement either directly on the ground or on obstacles. Coupling a rain-out model with the HEM approach is not an easy task as information about the diameter of liquid droplets and the size distribution is voluntary omitted. Consider a jet impinging on an obstacle located at a distance L in the positive x direction. In a grid cell (I, J, K) which is directly adjacent to the obstacle, the amount of liquid that rains-out at each time step is estimated via the following relation:

$$\begin{cases} m_{RO}(\vec{x}) = \sum_{q,k} Y_{q,k}^{l} m_k \quad if \quad T(\vec{x}) \le T_{NBP} \\ m_{RO}(\vec{x}) = 0 \quad if \quad T(\vec{x}) > T_{NBP} \\ \vec{x} = \left[x(I), y(J), z(K) \right] \end{cases} \tag{7}$$

Rain-out is authorized only if the temperature of the mixture inside the grid cell (I, J, K) is less or equal than the normal boiling point of the mixture. Mixture temperatures which are smaller or equal than the normal boiling point of the mixture indicate that liquid is evaporating and that thermodynamic equilibrium has been reached. The sum on the index k in Equation 7 is performed over all grid cells located at a distance less or equal than ℓ_{RO} from the wall. The characteristic length scale ℓ_{RO} for the rain-out process is defined as the product of the characteristic velocity (ϑ_{RO}) and characteristic time (τ_{RO}) scales for the rain-out process. The characteristic velocity for the rain-out process (ϑ_{RO}) is taken to be the local maximum velocity in regions of the flow where liquid is evaporating and thermodynamic equilibrium has been attained. This can be justified by the fact that the mass of liquid that deposits on the ground or on obstacles is expected to be contained inside the droplets having the largest diameters. These droplets have a large inertia, way larger than the inertia of fluid particles, and hence have an extended memory of their maximum velocities. Finally, the characteristic time τ_{RO} over which the rain-out process occurs is assumed to be the time needed by the flow to achieve a new thermodynamic equilibrium in the grid cell (I, J, K) adjacent to the wall. This time-scale is approximated by the time needed by the flow to bring new fluid particles to this grid cell. Appropriate source terms are integrated inside the transport equations for the mixture fractions and mixture enthalpy. The amount of liquid that is removed from the flow is injected inside the pool model.

In the case of liquid depositing on the ground and forming a pool FLACS solves the two-dimensional (2D) shallow water equations to calculate the behaviour of the pool. The assumption behind the shallow water theory is that the pool properties (temperature, velocity, etc.) are uniform across the thickness of the pool and, thus, are only a function of the horizontal coordinates. Therefore, the shallow water equations are an approximation of the equations of fluid motion, which is accurate when the thickness of the liquid pool is small in comparison with its horizontal dimensions. The advantage of using the 2D shallow water equations to calculate the pool spread and vaporization is that they account for the effect of terrain features (e.g., sloping, channels, etc.) or obstacles on the spread of the pool. The shallow water equations for the conservation of mass and momentum are:

$$\begin{cases} \dfrac{\partial h}{\partial t} + \dfrac{\partial h u_i}{\partial x_i} = \dfrac{\dot{m}_L - \dot{m}_V}{\rho_l} \\ \dfrac{\partial u_i}{\partial t} + u_j \dfrac{\partial u_i}{\partial x_j} = F_{g,i} + F_{\tau,i} \end{cases} \tag{8}$$

where $\dot{m}_L$ is the liquid spill rate into the pool and $\dot{m}_V$ is the rate of vaporization, and the terms on the right-hand side of the momentum equation represent the gravity and shear stress components. The rate of vaporization from the pool ($\dot{m}_V$) includes contributions from heat transfer from the substrate (e.g., ground or water), solar radiation and convective heat transfer from the air above the pool (Hansen et *al.*, 2007). The heat transfer components are factored into the energy equation, which is solved in terms of specific enthalpy:

$$\frac{\partial \theta}{\partial t} + u_i \frac{\partial \theta}{\partial x_i} = \frac{\dot{m}_L}{h}\left(\theta_L - \theta\right) + \dot{q}_c + \dot{q}_{rad} + \dot{q}_g + \dot{q}_{evap} \tag{9}$$

where $\dot{q}_c$ is convective heat transfer, $\dot{q}_{rad}$ is heat transfer to the pool from radiation, $\dot{q}_g$ is heat transfer to the pool from the substrate, and $\dot{q}_{evap}$ is heat loss due to evaporation. For cryogenic pools, heat transfer from the substrate is often the main source of heat input. In the FLACS pool model, heat transfer from a solid substrate (e.g., ground) is calculated as a function of position and time according to the semi-infinite solid heat transfer theory, assuming perfect contact between pool and substrate [8,23]. The 2D shallow water equations are solved at every time step and on the same computational domain as the atmospheric flow [1,8]. This allows the heat transfer from the ambient to be accounted for in a realistic and time-dependent manner.

3.0 SIMULATIONS AND RESULTS

3.1 Description of the experimental work

Un-ignited releases of liquid hydrogen were recently performed by HSL (Health and Safety Laboratory) in Buxton, UK, during the autumn of 2010. Four tests were conducted; tests 6 and 10 consisted of vertically downward release 100 mm above ground; test 7 was a horizontal release 860 mm above ground and test 5 was a horizontal release onto the ground. In this work we only consider tests 6 and 7. Liquid hydrogen was released at a fixed rate of 60 litres per minute for all the tests. The diameter of the orifice was 26.3 mm and the storage pressure was measured to be 2 bars (absolute pressure). The tests were conducted on a 32 m diameter concrete pad surrounded by hills as depicted on Figure 1. The wind speed was measured at the edge of the pad at a height of 2.5 m. The temperature was also measured but no information was available as regards to atmospheric stability. Temperatures within the cloud were measured at 30 positions.

3.2 Estimation of the source term

The mass flow rate is known and it is the same for all the tests but the volume fraction of gas at the exit orifice is unknown. Moreover, we assume that the temperature of the liquid hydrogen inside the storage device is the saturation temperature at the storage pressure. One can calculate the source term (mass flow rate, velocity, gas volume fraction) assuming that the hydrogen stays in the liquid phase until the exit orifice and flash, i.e. boils violently, at the exit orifice. This assumption does not seem to be valid because the mass flow rate which is obtained via the incompressible Bernoulli equation is one order of magnitude larger than the reported experimental mass flow rate. This observation may indicate that the flow is already two-phase at the exit orifice.

Figure 1. Picture of the test site

Our approach consists in assuming that the flow at the exit orifice is a homogeneous two-phase flow and that the temperature is the normal boiling point temperature. We then compute five different source terms based on five different assumed gas volume fractions at the exit. The simulations will be performed with these five source terms. This approach allows conducting a sensitivity study on the effects of the source term on the flow field.

The smallest gas mass fraction (source term ST1) is given by the calculation of the flash fraction based on a superheat degree of 3 K (i.e. the temperature difference between the storage temperature and the normal boiling point of hydrogen). The gas mass fraction is then gradually increased until we reach a pure gas flow at the orifice.

Table 1. Parameters of the 5 source terms used in the computations of Test-07 and Test-06

Source Term	Mass flow rate (kg/s)	Velocity (m/s)	Temperature (K)	Gas vol. fraction (-)	Gas mass fraction (-)
ST1	0.071	12	20	0.76	0.056
ST2	0.071	26	20	0.9	0.14
ST3	0.071	52	20	0.96	0.31
ST4	0.071	106	20	0.99	0.65
ST5	0.071	163	20	1	1

3.3 Results for Test-07

Test-07 was a horizontal release 860mm above ground. The wind speed was 2.9 m/s at a height of 2.5m, the wind direction was aligned with the positive X-direction and the atmospheric temperature was 11.5 ºC. We assumed a neutral Pasquill stability class. The grid resolution was 40 cm × 25 cm × 25cm close to exit orifice. Before investigating the effects of the different source terms on the flow field we first discuss the effect of O_2 and N_2 condensation on the temperature field. For each source term, Test-07 has been simulated with and without air condensation. Air condensation has an effect on the temperature field close to the exit orifice, where the temperature is less than the boiling point of N_2 and O_2. The effect of air condensation (slight warm-up of the jet; a maximum temperature difference of 10 ºC is observed) is restricted to a zone extending 20 exit orifice diameter downstream. The first sensor location is 1.5 m downstream of the source (equal to 60 exit orifice diameters), away from the zone of influence of air condensation. We then conclude that for Test-07 the process of air condensation can be neglected. A video of the release was recorded during the experiment. Figure 2 is a screen-shot of this video.

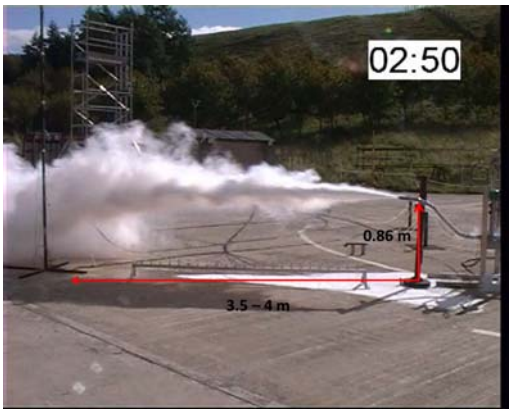

Figure 2 – Picture of the hydrogen jet for Test-07

Assuming that the white fog on Figure 2 is due to the presence of cold hydrogen we may directly compare the screen-shot with 2D-cut planes of the temperature field obtained from the simulations. Figure 3 shows 2D cut planes of the temperature fields obtained with the five source terms defined in Table 1. The jet starts to bend at approximately 3.5–4 m from the exit orifice (see Figure 2). The results obtained with the source terms ST3 and ST4 seem to be the closest ones to this experimental observation. It therefore means that more than 96 % in volume or 31 % in mass of the hydrogen released was in the gas phase at the exit orifice.

Figure 4 (left) presents a comparison between the predicted and observed minimum temperature at different locations inside the jet. We have chosen to report observed minimum temperatures rather than averaged temperatures because our simulations have been performed with the wind field aligned with the jet direction. In the experiments the wind field was likely fluctuating and possibly affected by the presence of the hills surrounding the test site. Therefore, our simulations – which do not account for those complex turbulent atmospheric features – would provide conservative temperature values. As it can be seen in Figure 4 (right), the experimental measurements showed a lot of fluctuations in reality due to variable turbulence levels.

It has been suggested above that simulations ST3 and ST4 seem to provide the closest predictions to reality. Predictions obtained with ST3 and ST4 are similar down to 4m (see Figure 4, left). Beyond 4m ST4 performs better than ST3 which may indicate that better far-field predictions would be obtained with ST4. Hence, Figure 4 (left) and the comparison between Figure 2 and Figure 3 allow stating that ST4 gives the best prediction of the observations. However, it is interesting to note that Figure 4 (left) shows that there is a smooth transition between ST2 and ST4 in terms of accuracy in the predictions as we move away from the exit orifice. The exact explanation for this observation is unknown. It is not clear whether it is due to a failure of the source term approach presented in Section 3.2 or to an overestimation of the negative buoyancy of the jet (with reference to ST2).

In the end, it can be mentioned that a statistical analysis of the temperature results could have been considered. However, many sensors are located outside the cloud, strong fluctuations are observed on the time-series and statistical analysis is usually based on concentrations data in atmospheric dispersion. Therefore, the authors think that profiles of minimum temperatures and temperature time-series provide more interesting inputs to the discussion.

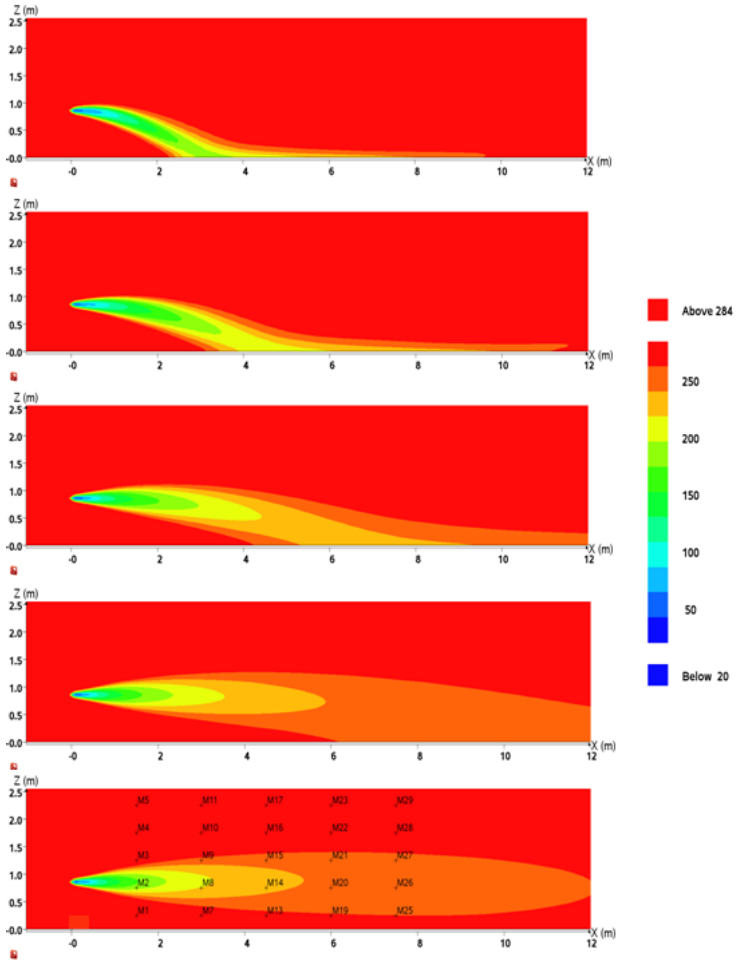

Figure 3. 2D cut-planes of the temperature field on the center-line axis of the jet obtained with different source terms. From top to bottom: ST1, ST2, ST3, ST4 and ST5

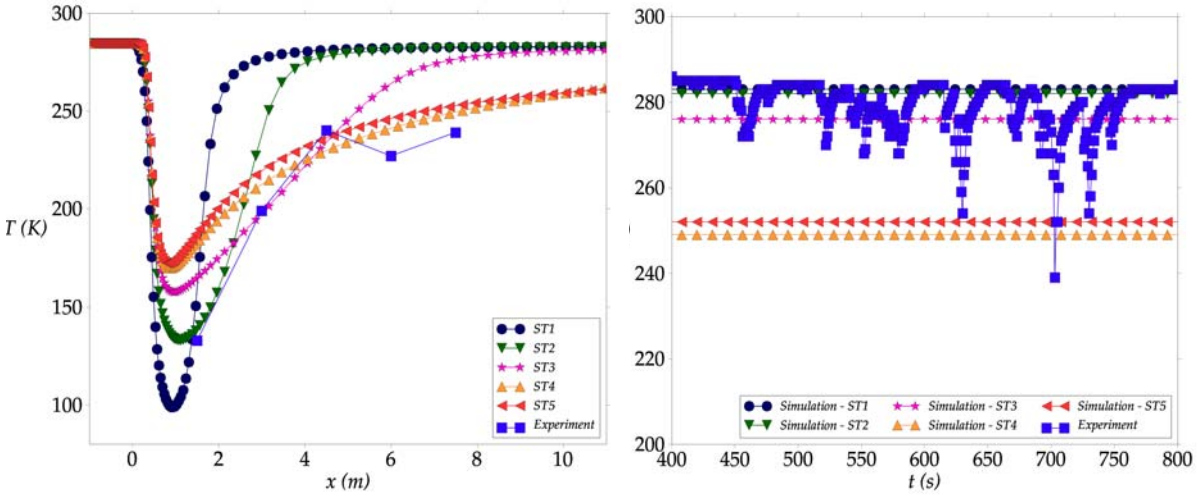

Figure 4. [Left] Minimum temperature as a function of distance for the horizontal release Test 07 0.75 m above the ground. [Right] Temperature time-series for Test-07 at sensor M26: X = 7.5 m; Z = 0.75 m

3.4 Results for test-06

The results for the Test-06 are now presented and discussed. Test-06 consisted of a vertically downward release 100mm above ground. The temperatures inside the hydrogen cloud were measured at the same positions than for Test-07. The wind speed was 3 m/s at a height of 2.5 m, the wind direction was aligned with the positive X-direction and the atmospheric temperature was 10 ºC. We assumed a neutral Pasquill stability class. The grid resolution was 25 cm × 25 cm × 10 cm close to exit orifice. We only consider the results obtained with the source terms ST4 and ST5. The source ST4 gives the most coherent results for Test-07 and the source term ST5 acts as a reference case for pure vapour release. We first investigate the effect of air condensation on the flow field. Figure 5 (left) shows a volume plot contour corresponding to the normal boiling point of N_2 (T = 77K). This contour plot shows the zone of the flow field where air (O_2 and N_2) is condensing. At the edge of the condensing zone a roll is developing. A similar roll is observed on the picture taken during the experiment (see Figure 5 - right). In our simulations the oxygen and nitrogen that change phase cannot deposit on the ground. Rain-out of liquid O_2 and N_2 is part of on-going modelling work. However, liquid hydrogen can rain-out on the ground but due to the very low liquid mass fraction at the source none of the hydrogen liquid is forming a pool on the ground.

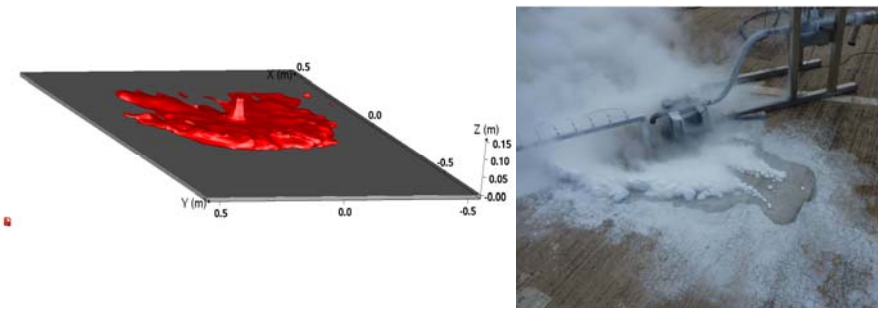

Figure 5. [Left] Temperature volume contour: T=77K. [Right] Picture from Test-06 showing ice depositing on the ground.

Figure 6 shows vertical profiles of temperature and vertical velocity 1.5 m downstream of the release point (it corresponds to the position of sensors M1, M2, M3, M4 and M5) with and without air condensation. For Test-06, by opposition to Test-07, air condensation has an effect on the flow field. It is worth noting that for both Test-06 and Test-07 the condensation process of oxygen and nitrogen is located close the release point. For Test-07 the condensation process is not able to affect the flow field passed the condensation zone but in the case of Test-06 the effect is felt way downstream of the condensation zone. Figure 6 illustrates the "air condensation" effect on the flow field, 1.5m downstream of the release point. It seems that the condensation of O_2 and N_2, by releasing energy close to the ground, generates an upward velocity that brings cold hydrogen gas to higher altitudes compared to the case without air condensation.

Time series of temperatures measured at two distances downstream are compared with the results of our simulations with air condensation. The two upper plots show the time series of temperature at sensors M1 (left) and M2 (right) located 1.5 m downstream of the release point. The two lower plots present the time series of temperature at sensors M7 (left) and M8 (right) located 3m downstream of the release point. At the two sensors M2 and M8 located at Z = 0.75 m the simulation with ST4 is not able to predict the presence of hydrogen. This could be explained by several factors, one factor being the poor representation of the actual atmospheric turbulence during the test. As mentioned in Section 3.1, the experimental site is surrounded by hills and obstructions are present on the test pad. These terrain features which are not represented in our simulations could be responsible for the generation of a more complex and intense atmospheric turbulent field increasing the mixing process between the cold hydrogen gas and the surrounding air.

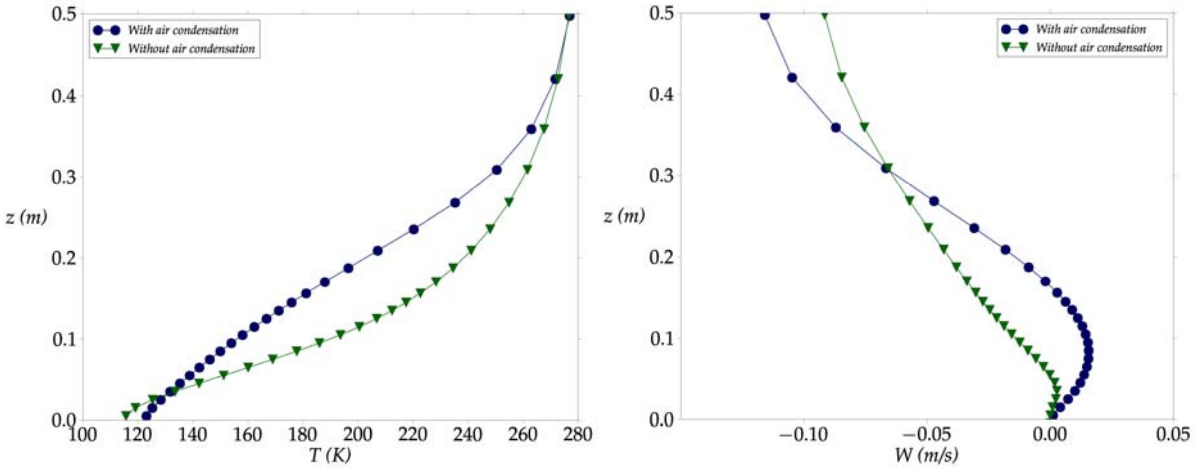

Figure 6. Vertical profiles of temperature and vertical velocity for Test-06 1.5m downstream of the release point.

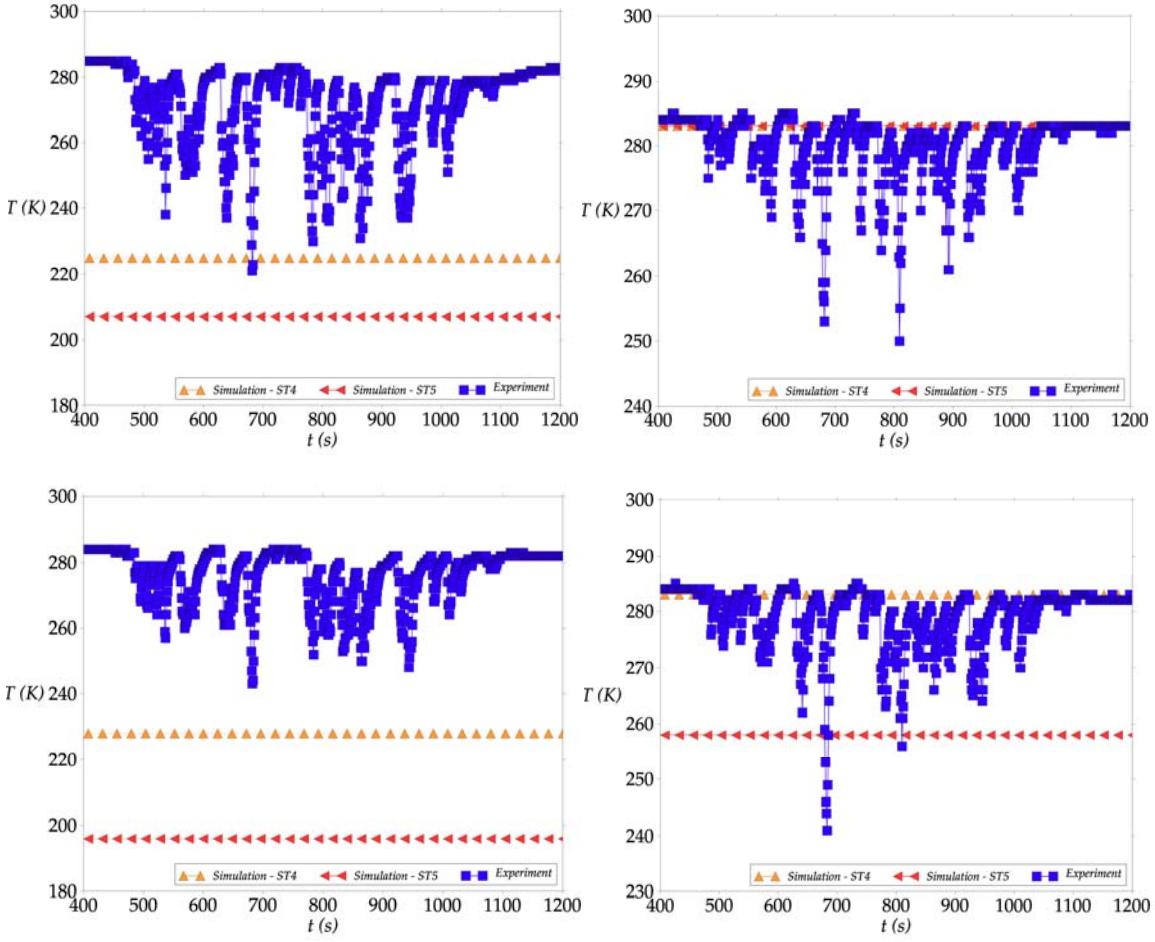

Figure 7. Temperature-time series for Test-06 at four locations. [Top] [Left] X = 1.5 m; Z = 0.25 m. [Right] X = 1.5 m; Z = 0.75 m. [Bottom] [Left] X = 3.0 m; Z = 0.25 m. [Right] X = 3.0 m; Z = 0.75 m.

4.0 CONCLUSIONS AND FUTURE WORK

The HSL liquid hydrogen Test-07 and Test-06 have been simulated with a new two-phase module implemented inside the CFD code FLACS. Test-07 consisted in a horizontal jet 0.86m above the ground whereas Test-06 was a vertical downward jet 0.1m above the ground. The storage pressure was measured to be 2 bars and the mass flow rate was reported to be 0.071 kg/s. Five different source terms based on five different assumed gas volume fractions at the exit were computed. The simulations were performed with these five source terms and a sensitivity study on the effects of the source term on the flow field was conducted. For Test-07, the comparisons between the experimental and predicted time-series of temperature at several positions downstream of the release point indicate that the source term ST4 is the most plausible source term. The condensation of oxygen and nitrogen has been modelled. No particular influence of air condensation on the flow field was noted for Test-07. However, for Test-06 a quite strong influence of air condensation on the temperature field was observed. It seems that the condensation of O_2 and N_2, by releasing energy, generates an upward velocity that brings cold hydrogen gas to higher altitudes compared to the case without air condensation. The hydrogen gas cloud becomes more buoyant.

Future work will mainly deal with three aspects: source term evaluation, better representation of the turbulence inside and around the two-phase cloud and implementation of models to take into account the effect of humidity. The sensitivity study performed on the source terms has shown that their influence on the flow field was not negligible. An accurate model to evaluate source terms for flashing releases is needed. The time series of temperature have shown that the CFD model was not able to predict the presence of hydrogen at several sensor locations (sensor M3 for Test-07 for example or sensor M2 for Test-06). A better representation of the surrounding atmospheric turbulence in connection with a more detailed approach for the modelling of two-phase flows may help in obtaining better results. An Euler-Lagrange method to model two-phase flows is being developed inside FLACS and will be used to simulate these liquid hydrogen releases in the near future. Finally, we have seen that the condensation of air could affect the dispersion of hydrogen by increasing the buoyancy of the cloud. The condensation of water vapour is therefore expected to also have an influence on the dispersion of the hydrogen cloud.

5.0 REFERENCES

1. Middha, P., Ichard, M. & Arntzen, B. (2010). Validation of CFD modelling of LH2 spread and evaporation against large-scale spill experiments. International Journal of Hydrogen Energy, 36: 2620-2627.
2. Statharas, J.C., Venetsanos, A.G., Bartzis, J.G., Wurtz, J. & Schmidtchen, U. (2000). Analysis of data from spilling experiments performed with liquid hydrogen. Journal of Hazardous Materials, 77: 57-75.
3. Witcofski, R.D. & Chirivella, J.E. (1984). Experimental and analytical analyses of the mechanisms governing the dispersion of flammable clouds formed by liquid hydrogen spills. International Journal of Hydrogen Energy, 9 (5): 425-435
4. Witcofski, R.D. (1981). Dispersion of flammable clouds resulting from large spills of liquid hydrogen. NASA Technical Memorandum 83131.
5. Verfondern, K., Dienhart, B., (1997). Experimental and theoretical investigation of liquid hydrogen pool spreading and vaporization, Int. J. Hydrogen Energy, 22, 649-660.
6. Venetsanos, A.G., Bartzis, J.G., (2007). CFD modelling of large-scale LH2 spills in open environment, Int. J. Hydrogen Energy, 32, 2171-2177.
7. Ivings, M.J., Jagger, S.F., Lea, C.J. & Webber, D.M. (2007). Evaluating vapour dispersion models for safety analysis of LNG facilities. The Fire Protection Research Foundation.
8. Hansen, O.R., Gavelli, F., Ichard, M. & Davis, S. (2010). Validation of FLACS against experimental data sets from the model evaluation database for LNG vapour dispersion. Journal of Loss Prevention in the Process Industries, 23 (6):857-877.

9. Ichard, M., Hansen, O. R. and Melheim, J. A. (2009). Modelling of flashing releases around buildings, 90th AMS annual meeting, Phoenix, AZ, USA.
10. Ichard, M., Hansen, O.R., Melheim, J.A. (2010). Releases of pressurized liquefied gases: simulations of the Desert Tortoise test series with the CFD model FLACS, 16th Conference on Air Pollution Meteorology, Atlanta, GA, USA.
11. Launder, B.E., Reece, G.J. & Rodi, W. (1975). Progress in the development of a Reynolds-stress turbulent closure. Journal of Fluid Mechanics, 68 (3): 537-566.
12. Hjertager, B.H., Fuhre, K. & Bjørkhaug, M. (1986). "Spherical gas explosion experiments in a high-density obstructed 27 m3 corner". Report on large-scale experiments performed at Sund, Norway, September-October 1984 and March 1985. CMI Report No. 865403-3, Chr. Michelsen Institute, Bergen, Norway.
13. van den Bosch, C.J.H., Weterings, R.A.P.M., (1997). Methods for the calculation of physical effects due to the release of hazardous materials (liquids and gases), CPR14E, TNO Yellow Book, 3rd edition, TNO, The Hague, The Netherlands.
14. Han, J., Arya, S.P., Shen, S. Lin, Y.L., (2000). An estimation of turbulent kinetic energy and energy dissipation rate based on atmospheric boundary similarity theory, Tech. Rep. CR-2000-210298, NASA, USA.
15. Dharmavaram, S., Hanna, S.R., Hansen, O.R., (2005). Consequence analysis – Using a CFD model for industrial sites. Process Safety Progress, 24: 316-327.
16. Flaherty J.E. et al, (2007). Evaluation study of building-resolved urban dispersion models, Seventh Symposium on the Urban Environment, 10-13 September 2007.
17. Hanna S.R., Hansen O.R., Ichard M., and Strimaitis D., (2009). Computational Fluid Dynamics (CFD) model simulations of dispersion from chlorine railcar releases in industrial and urban areas, Atmos. Environ., 43: 262-270.
18. Hanna, S.R., Hansen, O.R., & Dharmavaram, S. (2004). FLACS CFD air quality model performance evaluation with Kit Fox, MUST, Prairie Grass and EMU observations. Atmospheric Environment, 38: 4675-4687.
19. Witlox, H.W.M., Harper, M., Oke, A., Bowen, P.J. & Kay, P. (2010). Sub-cooled and flashing liquid jets and droplet dispersion I. Overview and model implementation/validation. Journal of Loss Prevention in the Process Industries, xxx: 1-12
20. Bonnet, P., Bricout, P., Jamois, D. & Meunier, P. (2005). Description of experimental large scale two-phase release tests, INERIS report No. 41508.
21. Kukkonen, J., Kulmala, M., Nikmo, J., Vesala, T., Webber, D.M., Wren, T., (1994). The homogeneous equilibrium approximation in models of aerosol cloud dispersion. Atmos. Environ. Vol. 28, No. 17, pp. 2763-2776
22. Faeth, G.M. (1983). Evaporation and combustion of sprays. Prog. Energy Comb. Sci., 9:1-76
23. Incopera, F. P., deWitt, D. P. (1996). Fundamentals of heat and mass transfer. Wiley Ed.